ChemComm

COMMUNICATION

View Article Online
View Journal | View Issue

Cite this: *Chem. Commun.*, 2015, 51, 4048

Received 19th December 2014,
Accepted 5th February 2015

DOI: 10.1039/c4cc10158h

www.rsc.org/chemcomm

The sequential continuous-flow hydrothermal synthesis of molybdenum disulphide

Peter W. Dunne, Alexis S. Munn, Chris L. Starkey and Edward H. Lester*

Molybdenum disulphide (MoS_2) has been widely used as a catalyst and high temperature lubricant. It has been heavily researched recently as a graphene analogue and member of the so-called inorganic fullerenes. Here we report the first continuous flow hydrothermal synthesis of MoS_2. With fast reaction times and flexibility the continuous flow hydrothermal system allowed MoS_2 to be produced in a stepwise fashion, offering an insight into the mechanism involved. It has been found that the synthesis of MoS_2 proceeded *via* the sulphidation of molybdate anions to thiomolybdate species, which are transformed to amorphous MoS_3 by acidification in flow, before further hydrothermal treatment decomposes this amorphous precursor to tangled MoS_2 nanosheets.

Molybdenum disulphide, MoS_2, has come under intense scrutiny in recent years. While it has long been of interest for its catalytic properties[1] and applications in high temperature lubrication, it is its position as a graphene analogue[2] and member of the so-called "inorganic fullerenes"[3–5] and its potential in intercalation chemistry and battery materials[6–8] which have driven much of the recent research activity. Great strides have been made in the production of few-layer 2-dimensional nanosheets of MoS_2 through vapour deposition techniques and exfoliation from crystalline MoS_2.[9,10] Inorganic fullerene-like MoS_2 structures have been synthesised by various methods, including vapour phase reactions[5] and post-synthetic annealing of solution processed core–shell precursors.[3] Nanostructured and hierarchical MoS_2 materials for catalytic and electrochemical applications have also been produced by vapour deposition methods,[11] as well as hydrothermal processes, though the hydrothermal routes typically require a post-synthetic annealing step to induce crystallisation.[8,12] Hydrothermal routes to molybdenum sulphide are becoming more and more common as the potential of hydrothermal synthesis to produce wide-ranging products with size, shape and composition control has gained broader acceptance. Despite this, hydrothermal methods do suffer some drawbacks. Chief among these is the difficulty in monitoring and understanding reactions which are occurring in sealed vessels under high temperatures and pressures (indeed, hydrothermal reactions have been, unfairly, referred to as a "magic hat" from which various products are pulled[13]). While extensive synchrotron studies have permitted researchers to examine reactions *in situ* under such harsh conditions, our understanding of hydrothermal processes still relies largely on a combination of chemical knowledge and systematic investigations of reaction conditions. Continuous-flow hydrothermal synthesis (CFHS) was developed initially for the rapid production of metal oxide nanoparticles by mixing precursors with a preheated supercritical water or reagent stream,[14] CFHS is significantly faster (<5 s) than conventional batch hydrothermal processes. This allows many variables to be examined through reaction and reactor design in order to enhance our understanding of the processes and mechanisms involved in these otherwise impenetrable systems. As a continuous-flow process CFHS is also inherently scalable to industrially viable levels (lithium iron phosphate for example is produced in this way at thousands of tons per year by Hanwha Chemicals).

We have previously reported on the continuous flow hydrothermal synthesis of a range of metal sulphides, wherein the size and shape of many of the materials could be controlled by varying reaction temperatures and how the reagents were mixed in flow.[15] Here we extend this work to the synthesis of molybdenum disulphide tangled nanosheets through a series of reactions carried out in flow. The rapid nature of the CFHS technique, coupled with a modular reactor design, has allowed us to elucidate and control the steps involved in the hydrothermal production of molybdenum disulphide by a continuous, scalable process.

Our initial efforts to produce MoS_2 in a continuous flow system mirrored our earlier work on metal sulphide nanomaterials.[15] Using the counter-current continuous flow reactor developed at Nottingham, and described in detail elsewhere,[15,16] an aqueous stream of ammonium heptamolybdate, at 0.05 M concentration flowing at 10 mL min^{-1}, was mixed with an aqueous stream of thiourea, at 0.1 M concentration, which had been flowed

Department of Chemical and Environmental Engineering, University of Nottingham, University Park, Nottingham, NG7 2RD, UK. E-mail: Edward.Lester@Nottingham.ac.uk

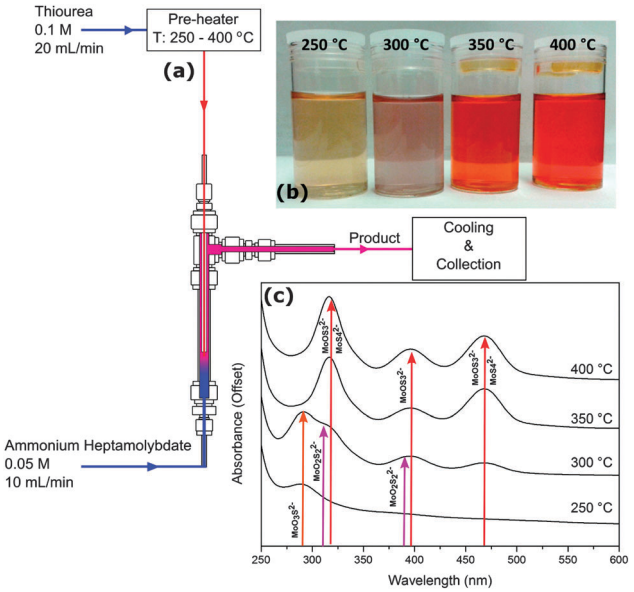

Fig. 1 Schematic of the counter-current reactor (a), photograph (b) and UV-vis spectra (c) of the thiomolybdate species formed by the reaction of molybdate with thiourea.

through a pre-heater at 20 mL min^{-1} at temperatures between 250 °C and 400 °C. A schematic of this reactor and the UV-vis spectra of the products obtained at various temperatures are shown in Fig. 1. No solids were obtained from this configuration at any temperature; however the solutions collected at the outlet of the reactor are deep orange to red in colour, indicative of sulphidation of the molybdate anions.[17] The UV-vis spectra show an increasing level of sulphidation with increasing reaction temperature, consistent with the step-wise mechanism:

$$MoO_4^{2-} + HS^- \rightarrow MoO_3S^{2-} \quad (1)$$

$$MoO_3S^{2-} + HS^- \rightarrow MoO_2S_2^{2-} \quad (2)$$

$$MoO_2S_2^{2-} + HS^- \rightarrow MoOS_3^{2-} \quad (3)$$

$$MoOS_3^{2-} + HS^- \rightarrow MoS_4^{2-} \quad (4)$$

It is worth noting that even at the highest pre-heater temperature of 400 °C the absorption maximum at 396 nm due to $MoOS_3^{2-}$ persists. This can be ascribed to the much slower rate of reaction for the final sulphidation reaction, relative to the preceding steps, however it has been shown previously that lowering the pH is an effective method of enhancing the rate of this reaction.[18]

In addition to speeding up reaction (4), acidification is known to precipitate the tetrathiomolybdate anion as amorphous MoS_3, itself a common precursor to MoS_2. Addition of small amounts of nitric acid to the obtained red solutions resulted in the precipitation of a dark brown solid (and gave a colourless supernatant) consistent with MoS_3. The reaction of MoS_4^{2-} with acid to yield MoS_3 involves reduction of the molybdenum. Despite the apparent formula, MoS_3 most likely consists of MoS_6 octahedra with the sulphurs of the shared faces forming disulphide units, giving a formula of $Mo^{IV}(S^{2-})(S_2^{2-})$, the exact structure and oxidation state remains slightly contentious. In order to produce MoS_3 with our

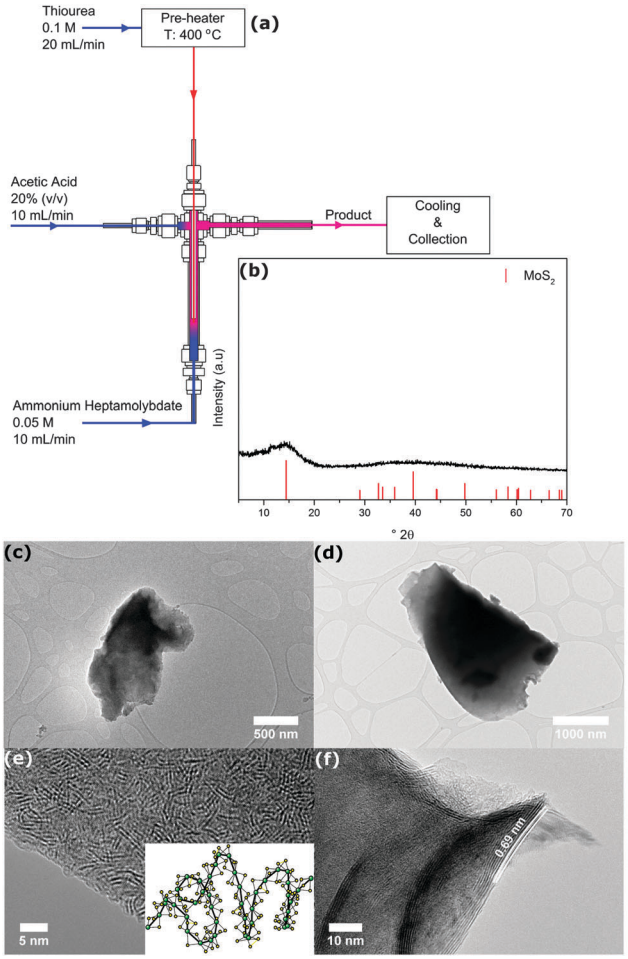

Fig. 2 Reactor for the production of MoS_3 by acidification of *in situ* generated thiomolybdates (a), and the XRD pattern (b) and HRTEM images (c–f) of the amorphous product (inset shows a possible structure as proposed by Hibble *et al.*).

fast continuous hydrothermal process, it was necessary to perform this acidification step in flow. An additional flow inlet to the reactor downstream of the initial mixing point was added to provide an acidic environment. Nitric acid creates too oxidising an atmosphere at the elevated temperatures employed, while the stainless steel construction of the reactor prohibits the use of hydrochloric acid as a reducing acid. As such acetic acid was chosen as a non-oxidising acid compatible with the stainless steel reactor. This reactor arrangement is shown in Fig. 2, along with the XRD pattern and TEM images of the brown solid obtained.

The XRD pattern of the product obtained from this reaction (recorded on a Bruker D8 Advance using Cu Kα radiation, λ = 1.5415 Å) is highly amorphous showing only a very broad peak centred at 14° 2θ and diffuse scattering at lower *d*-spacing. TEM images show the product consists of large micron-sized amorphous chunks. High resolution imaging reveals a highly disordered structure, seemingly comprised of tangled chain segments, consistent with the structural model proposed by Hibble *et al.*[19] on the basis of RMC modelling of neutron diffraction data. Some small isolated regions of the sample also exhibited a layered structure close to that expected of MoS_2, with interplanar

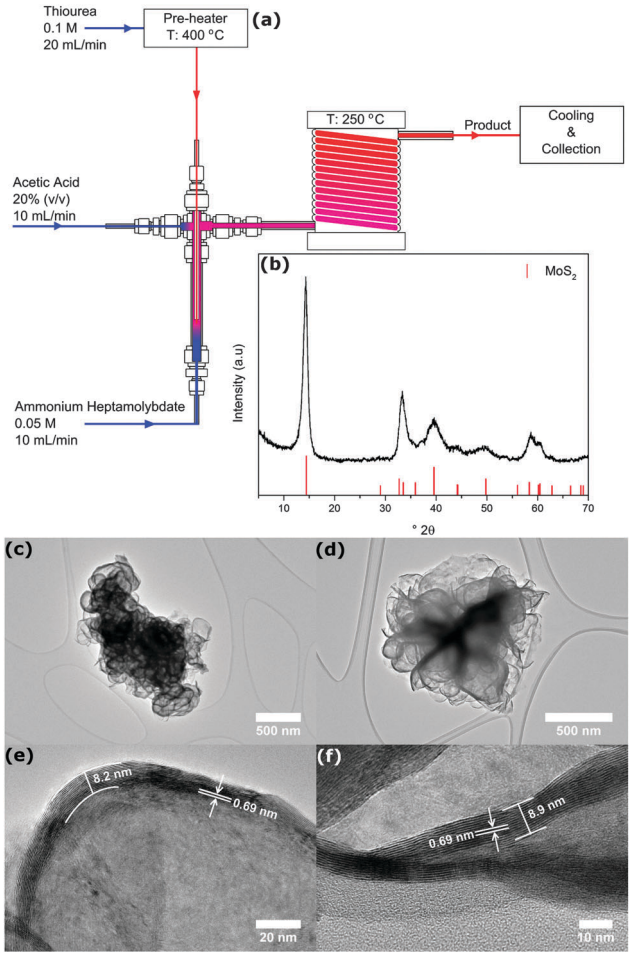

Fig. 3 The final reactor design for the production of MoS_2 by further hydrothermal treatment of MoS_3 (a), and the XRD pattern (b) and HRTEM images (c–f) of the crystalline MoS_2 product.

spacings of 6.9 Å, suggesting that at the elevated temperatures within the reactor some partial transformation of MoS_3 to MoS_2 has occurred, as has previously been suggested based on *in situ* EXAFS observations on the decomposition of tetrathiomolybdate to MoS_2.[20]

In order to fully transform the precipitated MoS_3 to MoS_2 additional heating is required. Conventionally this is achieved by calcination under an inert atmosphere, post-synthesis. In order to transform the MoS_3 to MoS_2 in flow it was necessary to increase the residence time of the reactor such that the MoS_3 would be maintained at sufficient temperatures long enough to decompose to MoS_2. This was achieved by incorporating an additional heating unit between the reactor outlet and the cooling system, affording an additional residence time of $\sim$30 s at a set temperature of 250 °C, as shown in Fig. 3a. The XRD pattern of the black solid obtained from this reactor reveals it to be crystalline MoS_2, obtained at near quantitative yields. TEM images show the MoS_2 is present as large (1–2 μm) masses of tangled nanosheets. HRTEM images taken at the edges of these curled nanosheets show them to be as little as 10 nm in thickness, typically between 10 and 15 layers of MoS_2.

This work represents the first successful synthesis of MoS_2 by the scalable continuous-flow hydrothermal method. Further, the rapid nature of the CFHS method has allowed various stages of the synthesis process to be observed by isolation of intermediates at different stages of reaction, such that a general mechanism can be proposed:

$$MoO_4^{2-} + HS^- \rightarrow MoO_xS_{4-x} \quad (5)$$

$$MoO_xS_{4-x} + H^+ \rightarrow MoS_3 \quad (6)$$

$$MoS_3 \xrightarrow{\Delta} MoS_2 \quad (7)$$

This research demonstrates that continuous-flow hydrothermal reactor technology can be employed as a flexible technique, which can be adapted to provide new avenues towards industrially relevant and important materials, while at the same time offering insights into the chemical mechanisms involved.

The authors wish to thank Dr Mike Fay and the Nottingham Nanotechnology and Nanoscience Centre for the use of and assistance with their HRTEM facilities, and Mr Mike Wallis and the School of Pharmacy for access to the UV-vis spectrometer. This work is funded through the European Union's Seventh Framework Programme (FP7/2007–2013), grant agreement no. FP7-NMP4-LA-2012-280983, the SHYMAN project.

Notes and references

1 P. Grange and X. Vanhaeren, *Catal. Today*, 1997, **36**, 375–391.
2 H. S. S. Ramakrishna Matte, A. Gomathi, A. K. Manna, D. J. Late, R. Datta, S. K. Pati and C. N. R. Rao, *Angew. Chem., Int. Ed.*, 2010, **49**, 4059–4062.
3 E. Blanco, D. Uzio, G. Berhault and P. Afanasiev, *J. Mater. Chem. A*, 2014, **2**, 3325–3331.
4 Y. Feldman, G. L. Frey, M. Homyonfer, V. Lyakhovitskaya, L. Margulis, H. Cohen, G. Hodes, J. L. Hutchison and R. Tenne, *J. Am. Chem. Soc.*, 1996, **118**, 5362–5367.
5 X.-L. Li, J.-P. Ge and Y.-D. Li, *Chem. – Eur. J.*, 2004, **10**, 6163–6171.
6 M. Pumera, Z. Sofer and A. Ambrosi, *J. Mater. Chem. A*, 2014, **2**, 8981–8987.
7 P. Sun, W. Zhang, X. Hu, L. Yuan and Y. Huang, *J. Mater. Chem. A*, 2014, **2**, 3498–3504.
8 S. Hu, W. Chen, J. Zhou, F. Yin, E. Uchaker, Q. Zhang and G. Cao, *J. Mater. Chem. A*, 2014, **2**, 7862–7872.
9 J. N. Coleman, M. Lotya, A. O'Neill, S. D. Bergin, P. J. King, U. Khan, K. Young, A. Gaucher, S. De, R. J. Smith, I. V. Shvets, S. K. Arora, G. Stanton, H.-Y. Kim, K. Lee, G. T. Kim, G. S. Duesberg, T. Hallam, J. J. Boland, J. J. Wang, J. F. Donegan, J. C. Grunlan, G. Moriarty, A. Shmeliov, R. J. Nicholls, J. M. Perkins, E. M. Grieveson, K. Theuwissen, D. W. McComb, P. D. Nellist and V. Nicolosi, *Science*, 2011, **331**, 568–571.
10 W. Yin, L. Yan, J. Yu, G. Tian, L. Zhou, X. Zheng, X. Zhang, Y. Yong, J. Li, Z. Gu and Y. Zhao, *ACS Nano*, 2014, **8**, 6922–6933.
11 X. Wang, H. Feng, Y. Wu and L. Jiao, *J. Am. Chem. Soc.*, 2013, **135**, 5304–5307.
12 X. Chen and R. Fan, *Chem. Mater.*, 2001, **13**, 802–805.
13 P. Afanasiev, *C. R. Chim.*, 2008, **11**, 159–182.
14 T. Adschiri, K. Kanazawa and K. Arai, *J. Am. Ceram. Soc.*, 1992, **75**, 1019–1022.
15 P. W. Dunne, C. L. Starkey, M. Gimeno-Fabra and E. H. Lester, *Nanoscale*, 2014, **6**, 2406–2418.
16 B. J. Azzopardi and E. H. Lester, WO 2005077505 A2, 2005.
17 S. H. Laurie, *Eur. J. Inorg. Chem.*, 2000, 2443–2450.
18 B. E. Erickson and G. R. Helz, *Geochim. Cosmochim. Acta*, 2000, **64**, 1149–1158.
19 S. J. Hibble and G. B. Wood, *J. Am. Chem. Soc.*, 2003, **126**, 959–965.
20 R. I. Walton, A. J. Dent and S. J. Hibble, *Chem. Mater.*, 1998, **10**, 3737–3745.

